Journal of Power Sources 196 (2011) 5945–5950

Contents lists available at ScienceDirect

Journal of Power Sources

journal homepage: www.elsevier.com/locate/jpowsour

Silicon-oxycarbide based thin film anodes for lithium ion batteries

J. Shen [a,1], R. Raj [a,b,*]

[a] Department of Mechanical Engineering, University of Colorado at Boulder, Boulder, CO 80309-0427, United States
[b] PDC Energy, LLC, Louisville, CO, United States

ARTICLE INFO

Article history:
Received 10 January 2011
Received in revised form 23 February 2011
Accepted 24 February 2011
Available online 6 March 2011

Keywords:
Silicon oxycarbide
Lithium ion batteries
Anodes
Thin films

ABSTRACT

We show that anodes made by depositing thin films of polymer-derived silicon oxycarbide (SiCO) on copper have properties that are comparable to, or better than that of powder-based SiCO anodes. The great advantage of the thin film architecture is its simplicity, both in manufacturing and in application. The films are produced by spraying a film of the liquid polymer-precursor on copper, and then converting it into SiCO by heating at ~1000 °C; at this point they are ready for constructing electrochemical cells. They show a capacity of ~1000 mA h g^{-1}, 100% coulombic efficiency, good capacity at very high C-rates, and minimal fading at ~60 cycles. However, if the films are thick they delaminate due to the volume change as lithium is cycled in and out. The transition from thin-film to thick-film behavior occurs when the SiCO films are approximately 1 μm thick. An analytical method for estimating this transition is presented.

1. Introduction

Graphite is the standard anode material for today's lithium ion batteries [1]. Graphite has a theoretical capacity of 371 mA h g^{-1}. These anodes are made by mixing graphite powder, a conducting agent (usually carbon black), and a binder in a 80–10–10 mixture, and screen printing the slurry on to a copper sheet. This structure is then baked before assembling it into an electrochemical cell.

The discovery that crystalline silicon has a capacity greater than 4000 mA h g^{-1} has spurred investigations into new materials for anodes [2]. However, silicon suffers from a huge volume expansion upon lithium intercalation, which results in fracture and fading in just a few cycles.

Recently a new material, polymer-derived silicon oxycarbide (SiCO) has drawn interest as an anode constituent [3,4]. In many ways SiCO represents a new paradigm in the science and technology of anodes. They are processed from off-the-shelf liquid precursors belonging to the siloxane family by a simple crosslinking and heat-treating process. They have a pseudo-amorphous, polymer-like network structure of atoms that is constituted from Si, C and O. The network is 'open', having a density that is two thirds that of crystalline materials. The open structure facilitates fast diffusion of lithium, which enables higher power densities than graphite or silicon. They show good cyclic stability, and chemical durability. However, while their *reversible* gravimetric capacity is nearly three times that of graphite, they do suffer from a high first cycle loss (ICL) which can be up to 35% of the first cycle capacity. The second drawback is the relatively large hysteresis. The discharge voltage for the SiCO anodes lies in the 0.8–1 V range which reduces the cell voltage by this amount when delivering power. Despite these shortcomings the polymer-derived materials represent a new class of anode materials. Their polymeric structure and chemistry is expected to evolve into new compositions and nanostructure that should be able to overcome the ICL and hysteresis.

Polymer-derived SiCO materials are processed from liquid organic precursors. The liquid is crosslinked into a hard epoxy-like material at 150–400 °C. It is then pyrolyzed at 800–1000 °C in an inert atmosphere to obtain the material that is used in anodes. Until now anodes from SiCO have been made by crushing the epoxy into a powder (before it is pyrolyzed) and then following the same procedure as used for constructing anodes from graphite powder, that is, mixing with a conducting agent and a binder in the 80–10–10 ratio, screen printing this slurry on to a copper sheet, and baking prior to assembling the electrochemical cell. In this article we show that this procedure can be greatly simplified by depositing a thin film of the liquid precursor directly on the copper sheet, pyrolyzing it at 1000 °C, and then using this architecture as the anode without any further processing. The properties of the thin film anode are comparable to, or better than that of powder-based SiCO anodes.

2. Experimental methods

The SiCO films were prepared in a pulsed liquid-injection reactor, which has been described in detail elsewhere [5,6]. In brief, the liquid precursor is sprayed into a hot wall reactor. The sam-

* Corresponding author. Tel.: +1 303 492 1029; fax: +1 303 492 3498.
E-mail address: rishi.raj@colorado.edu (R. Raj).
[1] Present address: School of Materials Science and Engineering, Henan University of Technology, Zhengzhou 450001, PR China.

0378-7753/$ – see front matter © 2011 Elsevier B.V. All rights reserved.
doi:10.1016/j.jpowsour.2011.02.091

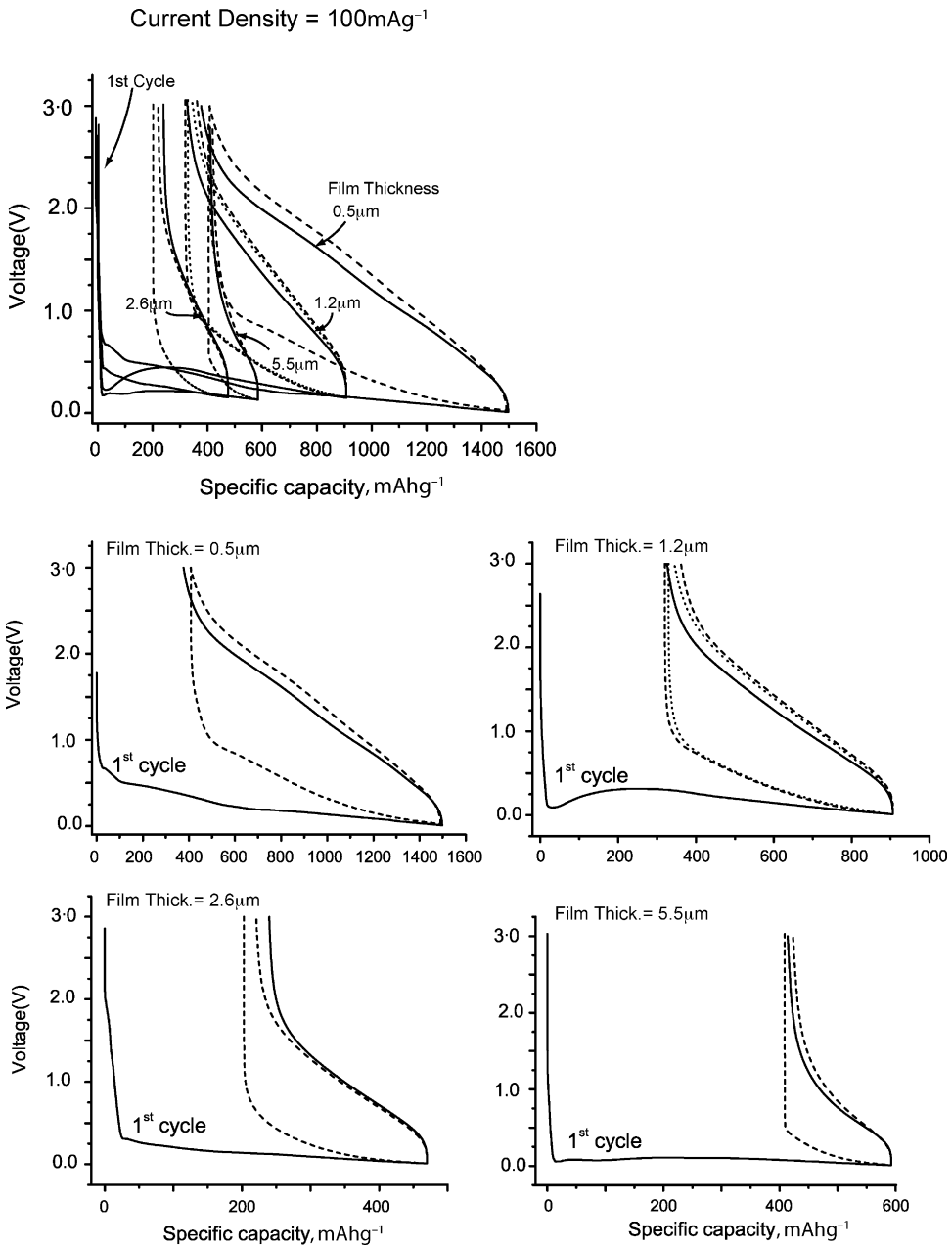

Fig. 1. The first two or three insertion–extraction cycles of Li into the anodes with films of different thicknesses. The 0.5 μm film performs better than, the 1.2 μm film is comparable to, while the thicker films perform worse than the powder-based SiCO anodes.

ple is heated with infrared halogen lamps encased within quad elliptical reflectors (Research Inc., Minneapolis, MN). The radiation furnace permits a rapid change in temperature. The reactor is continuously pumped with a rotary mechanical pump. The liquid is injected into the reactor by a pulsed mechanism that employs two valves connected in series with a small space between them to hold the volume of the liquid that is injected into the reactor. This mechanism serves two purposes: first, it controls the volume of liquid that is to be introduced into the reactor, and second, it serves as a buffer to isolate the low pressure within the reactor from the ambient pressure (the liquid supply reservoir is held at ambient pressure). The pulsed mechanism works in the following way: (i) the valve on the reactor side is closed, and the upstream valve is opened to fill the in-between space with the liquid; (ii) the upstream valve is closed and the reactor valve is opened to allow the liquid to spray into the reactor through an ultrasonic nozzle. The liquid deposited on the substrate is crosslinked before injecting the next pulse. Several such cycles may be used to build up the film to the desired thickness. The pressure in the reactor varies with time, being high when the pulse is injected and then decaying during the dead period when the film is being heat-processed.

The injected liquid consisted of 1 wt.% dicumyl peroxide in 1,3,5,7-tetramethyl-1,3,5,7-tetravinylcyclotertrasilosane (TTCS, Gelest, PA) diluted to 10% concentration in tetrahydrofuran (THF). The injected mixture was crosslinked at 180 °C. A pulse period of 1.5 min was used to polymerize the deposited precursor. The thickness of the films was varied by changing the total number of injections from 5 to 15 pulses. Then, the substrate was heated to 400 °C to complete the crosslinking, followed by heating at 1000 °C for 1 h to convert the polymer into SiCO. All processing was done inside the reactor without exposing the film to atmosphere. Argon was used as the flushing gas for cleaning the injector nozzle after every few pulses.

The anodes prepared by the above process were assembled into half-cells without any further processing. The half-cells consisted of lithium metal as the counter electrode, a polymer separator saturated with the liquid electrolyte, and the anode, in a coin cell configuration, having an electrode diameter of 1.56 cm. The electrolyte in these half-cells was a 1 M $LiPF_6$ solution in ethylene carbonate (EC) and dimethyl carbonate (DMC), in equal volumetric content. A trilayer of polypropylene and polyethylene was used as the polymer separator (from Celgard).

The electrochemical experiments were carried out with a battery tester (BT-2000, Arbin Instruments). The cut-off potentials of the half-cell were set between 0.01 V and 3 V. The nominal currents for lithium insertion and extraction were 100 mA g^{-1}. Five different film thicknesses corresponding the SiCO weight of 0.20 mg, 0.46 mg, 0.54 mg, 1.0 mg and 2.1 mg were evaluated. Assuming the nominal density of the SiCO to be ~2.0 g cm^{-1}, these weights correspond to a film thicknesses of 0.5, 1.2, 1.4, 2.6 and 5.5 μm, respectively.

3. Results and discussion

3.1. Cell performance

The first set of electrochemical measurements were made by inserting and extracting lithium at a current density of 100 mA g^{-1}, and measuring the voltage relative to pure lithium metal. The data shown in Fig. 1 closely resemble the results nominally obtained from powder-based SiCO anodes, but only when the film is ~1 μm thick. In thicker films the ICL increases, while the reversible capacity decreases steadily as the thickness is increased. For example, the 0.5 μm film has a reversible capacity of 1100 mA h g^{-1}, and an ICL of 27%. For the 1.2 μm film the ICL is increases to 33% and the reversible capacity declines to 600 mA h g^{-1}. For thicker films the performance deteriorates quickly to an ICL of 46% and a reversible capacity of 255 mA h g^{-1} for the 2.6 μm film, and, then, to an ICL of 67% and a reversible capacity of only 200 mA h g^{-1} when the film thickness increases to 5.5 μm. The reason for the decline in capacity with film thickness, as will be explained later, is attributed to the delamination of the films from the copper substrate upon Li cycling.

The reversible capacity of 1100 mA h g^{-1} and an ICL of 27% are slightly better than the values that were obtained for powder-based anodes, where, typically, the values were 800–900 mA h g^{-1} and an ICL of 30–35% [3].

In the next set of experiments the capacity of the cells was measured at higher current densities. As explained in an earlier publication the *C*-rates can be measured in two ways, by dividing the current density by the theoretical capacity of the anode material (for example 371 mA h g^{-1} for graphite) or using the as-measured capacity at a given current density. The first method is appropriate for crystalline materials where the Li forms a stochiometric compound with the anode host which gives a precise definition to the theoretical capacity. In the case of SiCO materials, which are amorphous, it is not possible to prescribe such an upper bound value; instead the capacity changes continuously with composition and processing conditions. Therefore the *C*-rate in the present experiments is defined by the following equation [3]:

$$n\bar{C}, \quad \text{where} \quad n = \frac{i_a}{q(i_a)}\text{h}^{-1} \tag{1}$$

where i_a is the current density in mA g^{-1}, and $q(i_a)$ is the capacity in mA h g^{-1} measured at this current density. The results for three film thicknesses are shown in Fig. 2. These experiments were carried out with symmetric cycles such that the insertion and the extraction current densities were equal. In the conventional approach the *C*-rate effect is measured with asymmetric cycles where Li is inserted into the anode at a slow rate, and then extracted at higher current densities. The results presented in Fig. 2 are, therefore, conservative with respect to the conventional *C*-rate testing procedure. The symmetric cycles were used in order to reduce the experimental time scale to manageable levels. While all films show a decline in capacity with higher *C*-rates, the thinner films show a stable behavior at very high *C*-rates. The 0.5 μm film approaches a capacity of ~150 mA h g^{-1} at *C*-rates of up to 150 h^{-1}. This behavior has also been seen in powder-based anodes of SiCO [7].

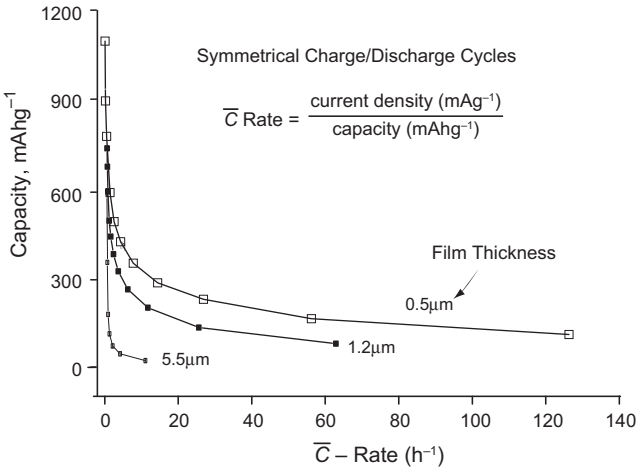

Fig. 2. The change in capacity with charging rate using symmetrical insertion–extraction cycles.

Next, the coin cells were cycled with symmetrical insertion–extraction cycles at a current density of 100 mA g^{-1} to determine the susceptibility of the anode films to fading and to measure changes in the coulombic efficiency. These results are given in Fig. 3. Interestingly the coulombic efficiency of the film anodes was always almost exactly 100% for all cases and for all cycles. This result is in sharp contrast to the powder-based anodes where the coulombic efficiency varies between 95% and 100% [3]. The main difference between the thin-film anodes and powder-based anodes is the way in which the electrons are transported from the active anode material to the current collector. In the thin-film architecture the anode is in intimate contact with the

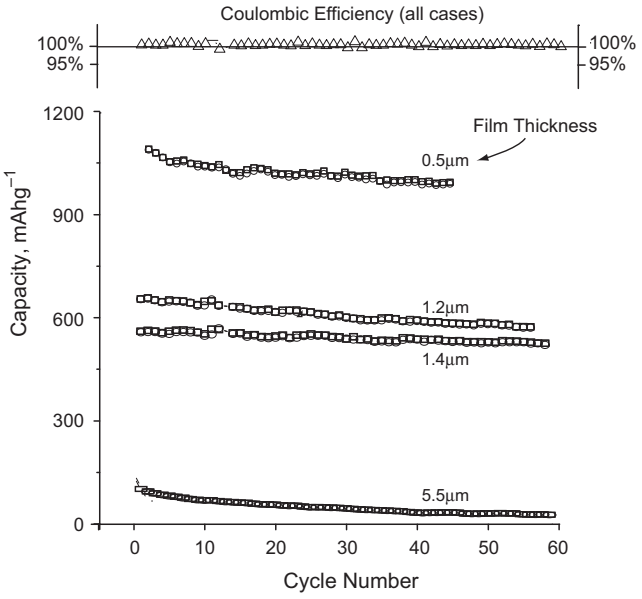

Fig. 3. The cyclic stability and coulombic efficiency of the anodes.

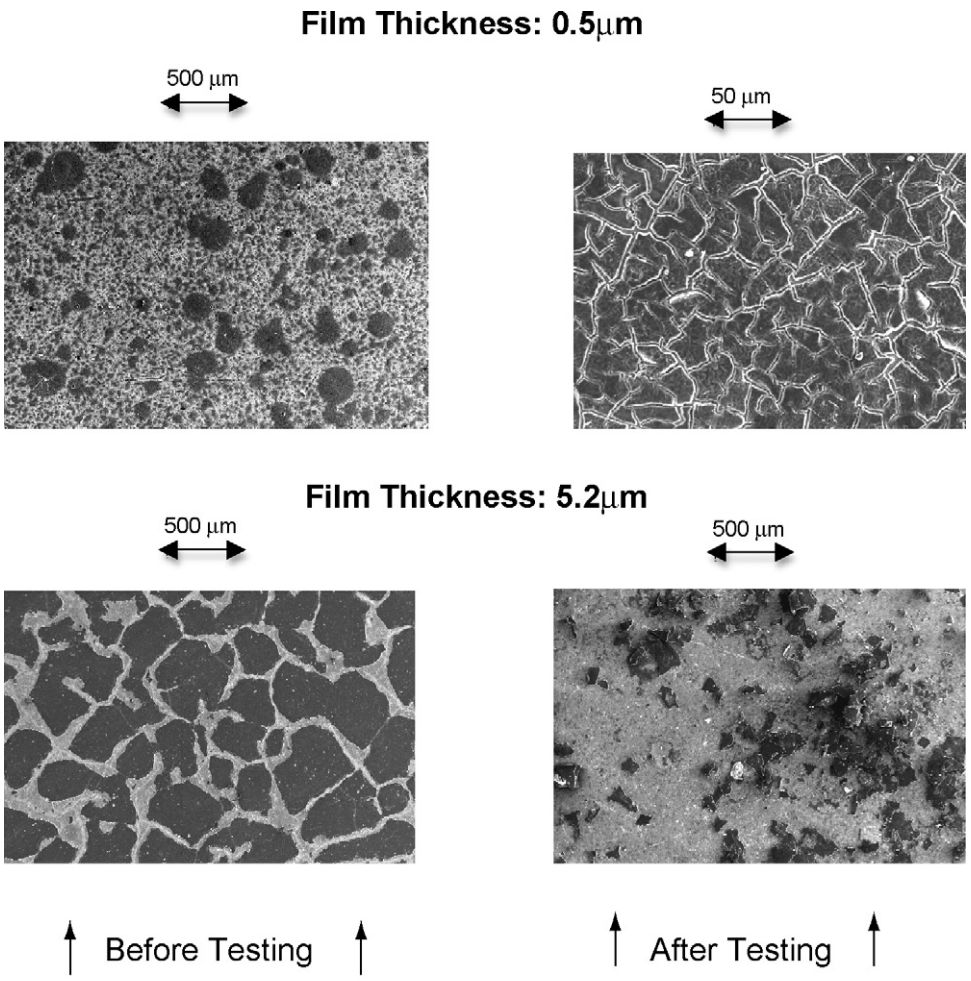

Fig. 4. The microstructure of the films before and after testing. Thicker films delaminate upon cycling while the thin films remain intact. The bright areas on the surface reflect bare copper while the dark areas represent SiCO coverage.

copper current collector. In the powder architecture a conducting agent, such as carbon black, is used to create a pathway for the electrons to be transported from the surface of the anode particle to the copper current collector. It is possible that the lower coulombic efficiency of the powder architecture arises from the variability in the pathways for the electrons to travel from the surface of the anode particles to the current collector through the conducting agent.

The data presented in Fig. 3 show the cyclic stability of the capacity, extending up to 60 cycles. The stability is quite good for the ~1 μm or thinner films but poor for the films that were several micrometers thick. The reason for this difference in performance became clear from the examination of the microstructure of the films before and after testing.

3.2. Microstructural observations

Scanning electron micrographs of the 0.5 μm film and the 5.2 μm film before electrochemical testing and after cycling are shown in Fig. 4. The pristine films are shown on the left, and postmortem micrographs on the right. The bright contrast in the micrographs represents free copper surface, while the dark areas are covered with SiCO.

The micrographs from the pristine films, on the left, which are taken at the same magnification, show a difference between the thin and the thick films. While the thin film has fine "mud" cracks that are closely spaced and barely visible, the thick film shows widely spaced cracks in the film with the copper underneath reflecting through the width of the cracks. The cracks in the film develop because of the constraint to the shrinkage in the film that occurs when it is pyrolyzed at ~1000 °C (the density of the pyrolyzed SiCO is approximately 2 g cm^{-3}, whereas it is only ~1 g cm^{-3} for the crosslinked polymer [8]). In the films this shrinkage is accommodated by the in-plane contraction which leads to the cracks seen clearly for the thick film. Indeed the spacing of these cracks is expected to be related to the thickness of the films by the following equation [9]:

$$\lambda = \frac{\pi h \sigma_F}{\tau_{\text{int}}} \tag{2}$$

where λ is the spacing between the cracks, h is the thickness of the film, σ_F is the tensile fracture stress of the film, and τ_{int} is the effective yield stress of the copper–SiCO interface. Note that the equation predicts that the crack spacing would increase linearly with the film thickness, in agreement with the observations. In Eq. (2), the fracture stress and the interfacial yield stress are material parameters.

The micrographs on the right hand side in Fig. 4 show the state of the film after full scale testing as described in the previous section. The remarkable difference is that while the thin films remain in contact with the copper substrate, the thick films have mostly delaminated and fallen away when the electrode was extracted from the coin cell for SEM examination (the dark spots is all that

remains of the SiCO films on the surface). The most likely explanation is the elastic strain produced in the film when Li is cycled in an out of the SiCO. The volume expansion associated with Li insertion, which will produce this strain, has not yet been directly measured. The probability of delamination depends on the work done in the fracture of the interface, and the strain energy available in the film to drive such fracture. The work of fracture is equal to the product of the fracture energy per unit area times the area of the interface that delaminates; thus it is proportional to the in plane interfacial area of the segment that separates from the copper substrate. The driving force for fracture is related to the strain energy per unit volume of the film multiplied by the volume of the film-segment. The latter is equal to the area of the film-segment multiplied by the film thickness. Therefore, as the film becomes thicker the driving force for delamination increases while the work of fracture remains constant. The threshold fracture condition is reached when the strain energy becomes greater than the work of fracture. This argument leads to the following equation for the critical thickness of the film for fracture:

$$h_c = \alpha \frac{2\gamma_F}{\varepsilon_{Li}^2 E} \tag{3}$$

The fracture condition is that $h \geq h_c$. Here α is a geometry parameter of order unity, γ_F is the fracture energy of the interface in units of J m^{-2}, E is the Young's modulus of the film (i.e., SiCO) and ε_{Li} is the linear strain produced in SiCO when it is saturated with Li (the volume strain being equal to $3\varepsilon_{Li}$). For an order of magnitude calculation let us assume that $\alpha = 1$, $\gamma_F \approx 5$ J m^{-2}, and assume that $\varepsilon_{Li} \approx 0.03$ and the nominal value for the Young's modulus, $E = 50$ GPa [8]. Substituting these values in to Eq. (3) gives that $h_c = 0.3$ μm, which is within an order of magnitude of our experimental observations.

3.3. Diffusion of Li in SiCO

The underlying concept behind the thin film experiments was to measure the diffusion coefficient by systematically changing the film thickness. We had assumed that the effective diffusion distance for Li in the SiCO films would be controlled by the thickness of the films. It would then have been possible to determine the diffusion coefficient by measuring the change in the relaxation time for voltage recovery when a short charge or discharge of lithium is followed by the measurement of the time dependent change in the voltage under open circuit conditions [10,11]. The measured EMF is related to the surface activity of Li in SiCO via the Nernst equation. Thus as diffusion evens out the concentration of Li in the film the voltage profile would measure this relaxation time, from which it would be possible to elicit a value for the diffusion coefficient. In general the diffusion coefficient and the relaxation time are related to the rate controlling length dimension in the microstructure by the equation:

$$nD_{Li}t = \beta L^2 \tag{4}$$

here $n = 2$, 4, or 6, depending on whether the flow fields for diffusion are commensurate with one, two or three dimensions, respectively, D_{Li} is the diffusion coefficient for Li in the host material, t is the characteristic relaxation time, and L is the microstructural length scale that is expected to control the diffusive relaxation. Again, β is a non-dimensional adjustable parameter which, in the first instance, may be assumed to be unity.

The application of Eq. (4) requires a visualization of the flow field of Li diffusion in the SiCO film. We had assumed that in the present design of experiments diffusion would occur through the thickness of the film. In this situation, the flow is unidimensional, so that $n = 2$,

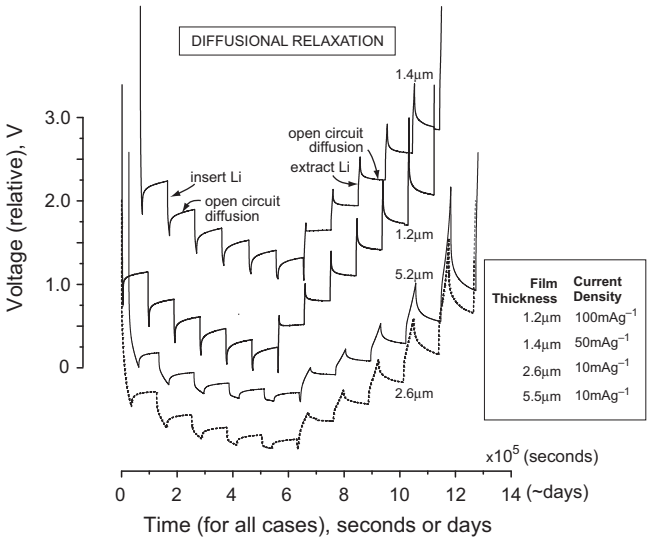

Fig. 5. The EMF relaxation profiles for diffusive relaxation experiments.

and the characteristic diffusion distance will be equal to the thickness of the film, that is $L \approx h$. We had hoped that by varying h, we could unequivocally show that the relaxation time would increase as h^2, thereby giving credible values for the diffusion coefficient. Since the thickness of the film varies over a factor of ten, a hundred fold change in the relaxation time was expected. However, the results, which are reproduced in Fig. 5, were entirely incongruent with this prediction. The data show the relaxation behavior for several films at many steps in the charging cycle (the experiments were carried out by a short charging or discharging period, at a certain current density, followed by measurement of the relaxation time by the change in the EMF under open circuit). In nearly all instances the relaxation times appear to range from 1 to 5 h, despite a five fold change in the film thickness. Clearly, the thickness of the film does not control the effective diffusion distance in the microstructure.

The results in Fig. 5 are explained by the schematic in Fig. 6. We suggest that the diffusion flow field is not in the thickness direction but rather in the biaxial, in-plane directions. The Li-ions are reduced to Li at the triple junction, where SiCO, copper and the electrolyte meet. The Li injected at the triple junction then flows inwards towards the center of the film segment, as illustrated by the flow-field arrows in the figure. In this scenario the effective diffusion distance is proportional to the segment size, that is, the spacing between the cracks in the film, shown as λ in Fig. 6.

4. Summary and conclusions

(a) Thin films of SiCO perform as well or better than powder-based anodes of the same material. The thin films can lead to significant simplification of the design and manufacturing of Li-ion batteries. The thin film design requires fewer steps in anode fabrication and battery assembly. For example conducting agents and polymer binders that are necessary in conventional powder-based anodes are no longer needed.

(b) The adherence of thin films to the copper anode collector is a significant issue in the design of the films. If the films are above a critical thickness, as described by Eq. (3), then they would tend to delaminate leading to fading capacity. In the current experiments films having a thickness of less than approximately 1 μm had good performance.

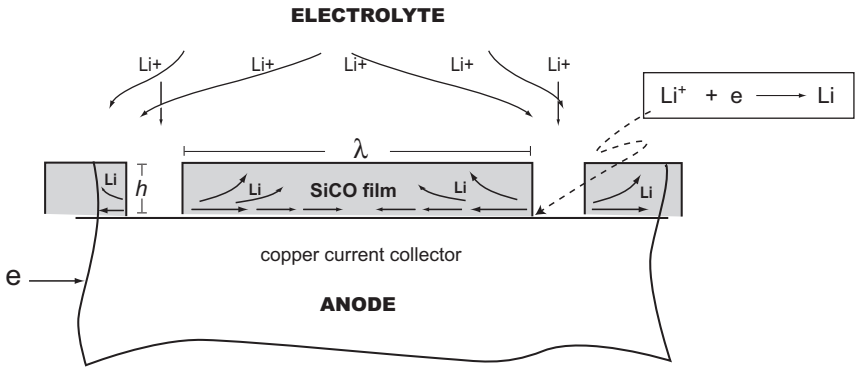

Fig. 6. A schematic of the expected diffusion field of Li into the SiCO films.

(c) The capacity, coulombic efficiency, and stability of the thin films were as good or exceeded the performance of powder-based SiCO anodes. The first cycle loss for thin films was smaller, about 25% of the first cycle capacity, as compared to ∼33% for the powder-based anodes. The coulombic efficiency of the films held steadfastly at 100%.

(d) The films exhibit 'mud-cracking', which originates from the shrinkage in the material as it converts from crosslinked organic to the SiCO ceramic phase. However, this phenomenon does not detract from the viability of the thin film architecture of the anode.

(e) Although there are as yet no measurements of the volumetric change in SiCO upon Li intercalation, the present experiments suggest that this volume expansion may be large enough to cause delamination of the films, causing a loss of capacity. However, these strains remain harmless if the film thickness is below a critical value, as given by Eq. (3).

(f) The measurement of relaxation times for Li diffusion suggest that the diffusion of Li into the SiCO film is likely to be controlled by diffusion parallel to plane of the film. The characteristic diffusion distance for this process is equal to the segment size of the film, as explained in (d) above, and is related to the diffusion coefficient by Eq. (4).

Acknowledgement

This research was supported by the Ceramics Program of the Division of Materials Research at the National Science Foundation, under grant no: 0907108.

References

[1] L. Lacroic-orio, M. Tillard, D. Zitoun, C. Belin, Chem. Mater. 20 (2008) 1212–1214.
[2] J. Graetz, C.C. Ahn, R. Yazami, B. Fultz, Electrochem. Solid-State Lett. 6 (2003) A194–A197.
[3] D. Ahn, R. Raj, J. Power Sources 196 (2011) 2179–2186, doi:10.1016/j.jpowsour.2010.09.086.
[4] P.E. Sanchez-Jimenez, R. Raj, J. Am. Ceram. Soc. 93 (2010) 1127–1135.
[5] S. Krumdieck, R. Raj, J. Am. Ceram. Soc. 82 (1999) 1605–1607.
[6] V.A. Versteeg, T.A. Avedisian, R. Raj, Method and apparatus for CVD using liquid delivery system with an ultrasonic nozzle, U.S. Patent No: 5,451,260, September 19, 1995.
[7] J. Shen, D. Ahn, R. Raj, J. Power Sources 196 (2011), doi:10.1016/j.jpowsour.2010.11.009.
[8] T. Cross, R. Raj, S.V. Prasad, T.E. Buchheit, D.R. Tallant, J. Am. Ceram. Soc. 89 (2006) 3706–3714.
[9] D.C. Agrawal, R. Raj, Acta Metall. Mater. 37 (1989) 1265–1270.
[10] C.J. Wen, B.A. Boukamp, R.A. Huggins, W. Weppner, J. Electrochem. Soc. 126 (1979) 2258–2266.
[11] D. Ahn, R. Raj, J. Power Sources 195 (2010) 3900–3906.